esa

ECOSPHERE

Incorporating biophysical gradients and uncertainty into burn severity maps in a temperate fire-prone forested region

Brian J. Harvey,[1,]† Robert A. Andrus,[2] and Sean C. Anderson[3]

[1]*School of Environmental & Forest Sciences, University of Washington, Campus Box 352100, Seattle, Washington 98195 USA*
[2]*Department of Geography, University of Colorado, Boulder, GUGG 110, 260 UCB, Colorado 80309 USA*
[3]*Pacific Biological Station, Fisheries and Oceans Canada, 3190 Hammond Bay Rd., Nanaimo, British Columbia V9T 6N7 Canada*

Citation: Harvey, B. J., R. A. Andrus, and S. C. Anderson. 2019. Incorporating biophysical gradients and uncertainty into burn severity maps in a temperate fire-prone forested region. Ecosphere 10(2):e02600. 10.1002/ecs2.2600

Abstract. As forest fire activity increases worldwide, it is important to track changing patterns of burn severity (i.e., degree of fire-caused ecological change). Satellite data provide critical information across space and time, yet how satellite indices relate to individual measures of burn severity on the ground (e.g., tree mortality or surface charring) and how these relationships change across biophysical gradients remain unclear. To address these knowledge gaps, we used Bayesian hierarchical zero-one-inflated beta (ZOIB) regression models with nearly 600 plots of individual field measures of burn severity distributed across the U.S. Rocky Mountains. We asked the following: How do three commonly used satellite indices of burn severity relate to individual field measures of canopy burn severity and forest-floor burn severity (Q1)? Then, using the highest ranked satellite index, how is reliability affected by biophysical gradients that can be captured in accessible geospatial data (e.g., latitude, slope) (Q2) and stand-structure data typically available only with field data (Q3)? The Relative differenced Normalized Burn Ratio (RdNBR) outperformed the differenced Normalized Burn Ratio (dNBR) and the Relative Burn Ratio (RBR) across canopy and forest-floor measures of burn severity, but differences among index performances were minor. Overall, indices performed better for field measures of canopy burn severity than for forest-floor measures. The relationship between RdNBR and individual field measures of burn severity changed across several biophysical gradients. For example, the same value of RdNBR corresponded to different field levels of burn severity depending on latitude, pre-fire forest structure, and pre-fire beetle outbreaks—and effects of biophysical gradients were often different for canopy vs. forest-floor measures of burn severity. We show that estimating field measures of burn severity using satellite indices can be improved by including biophysical information, but if variables that are difficult to obtain without field data (e.g., pre-fire beetle outbreak severity) are lacking, we suggest caution in interpreting satellite indices of burn severity across gradients of pre-fire biophysical conditions. Finally, using an example fire, we illustrate contrasting maps of burn severity that arise from differences in the relationship between individual field measures of burn severity and RdNBR after accounting for error in those relationships.

Key words: conifer forest; disturbance ecology; fire ecology; Landsat; normalized burn ratio (NBR); remote sensing; Rocky Mountains.

Received 28 September 2018; revised 13 December 2018; accepted 7 January 2019. Corresponding Editor: Lucas N. Joppa.

† **E-mail:** bjharvey@uw.edu

Introduction

Fire is a natural disturbance that is integral to the structure and function of many forests throughout the world (Attiwill 1994), with tens of millions of hectares (ha) burning each year. A warming climate is substantially increasing

wildfire activity (Moritz et al. 2012, Flannigan et al. 2013, Abatzoglou and Williams 2016, Westerling 2016), which will likely have profound ecological consequences for fire-prone forest ecosystems (Millar and Stephenson 2015, Johnstone et al. 2016). As such, accurately detecting components of fire regimes (i.e., the frequency, severity, and size of wildfires; Agee 1996) and how they may be changing with climate warming is a pressing scientific and societal need.

Widespread availability of satellite data collected since the mid-1980s has allowed for monitoring of wildland fires across expansive areas, bringing "big data" to bear on tracking changing fire regimes. A key fire regime metric that is often the focus of fire ecology research is *burn severity* (i.e., the degree of short-term ecological change caused by fire, typically measured by biomass lost or vegetation killed by fire, Keeley 2009, Morgan et al. 2014). Field and satellite remote sensing data have been used to assess burn severity since the mid-1990s (White et al. 1996, Patterson and Yool 1998, Lentile et al. 2005, 2006*a*, *b*) and have proliferated since the mid-2000s in the United States with the Monitoring Trends in Burn Severity program—a multi-year project supported by the U.S. Forest Service and Department of Interior, whereby all fires larger than 400 ha are mapped and cataloged online (Eidenshink et al. 2007). Researchers can access and download 30-m resolution images (derived from Landsat TM satellites) of burn severity for each fire in the dataset, which currently contains more than 20,000 individual fires. The value of such wall-to-wall mapping of burn severity for nearly all fires that burn each year is indisputably high, but like many instances of big data compilations, it is often hampered by a lack of on-the-ground field data to calibrate or validate satellite burn severity indices (Morgan et al. 2014, Kolden et al. 2015).

One key knowledge gap in tracking changes in fire regimes over space and time is understanding how satellite indices relate to individual components of burn severity (i.e., fire effects) on the ground (Morgan et al. 2014, Kolden et al. 2015, Smith et al. 2016). Two widely used indices of burn severity are derived from the Normalized Burn Ratio (NBR; Key and Benson 2005), which relates to chlorophyll content in plants, moisture, and surface char/ash: the differenced Normalized Burn Ratio (dNBR; Key and Benson 2005) and the Relative differenced Normalized Burn Ratio (RdNBR); the latter removes bias of pre-fire vegetation cover among locations and is therefore best suited for regional studies across different forest types (Miller and Thode 2007, Dillon et al. 2011, Cansler and McKenzie 2014). A mathematically simpler Relative Burn Ratio (RBR) has also been proposed and has shown promise in outperforming dNBR and RdNBR (Parks et al. 2014*a*). In short, by comparing differences between the near- and shortwave-infrared reflectance values (wavelengths of 0.77–0.90 μm and 2.09–2.35 μm, respectively) in pre- and post-fire Landsat satellite images, each of these NBR-derived indices generates a continuous index of burn severity across an entire burned landscape; greater values equate to greater change from pre- to post-fire and, therefore, greater burn severity. The relationship between field measures of burn severity and satellite measures of burn severity has been tested in many Northern Hemisphere forest ecosystems (Cocke et al. 2005, De Santis and Chuvieco 2007, Lentile et al. 2007, Miller and Thode 2007, Smith et al. 2007, French et al. 2008, Cansler and McKenzie 2012, Parks et al. 2014*b*). However, most existing field datasets used to calibrate and validate satellite indices of burn severity are composed of semiquantitative (ordinal) field data on burn severity (e.g., the Composite Burn Index, CBI; Key and Benson 2005), which are then typically converted to a single set of categorical burn severity classes for analysis (Cansler and McKenzie 2012); few studies have tested satellite indices against individual continuous field measures (Miller et al. 2009, Whitman et al. 2018). While instructive for quick field assessments that inform broad categories of burn severity, the typical use of CBI relies on user subjectivity and collapses many individually distinct metrics of burn severity into one value, thus inhibiting the ability of researchers to map individual components of burn severity across space and time (Morgan et al. 2014). Precise quantitative relationships between widely used satellite indices and field measures of individual components of burn severity (e.g., tree mortality or forest floor charring) have heretofore not been rigorously tested across wide swaths of fire-prone forests (Morgan et al. 2014, Kolden et al.

2015; but see Miller et al. 2009 for an example from California).

A second key knowledge gap that limits insights about how disturbance regimes may be changing is understanding whether the relationship between satellite and field measures of burn severity varies across gradients of geography, topography, and stand structure. Recent work has tested the effect of topography, climate, weather, and vegetation as drivers of burn severity (Birch et al. 2015, Kane et al. 2015, Harvey et al. 2016*b*), but how these variables affect the performance of satellite indices of burn severity remains unclear. For example, if the same level of satellite burn severity (e.g., RdNBR = 500) equates to different levels of fire-caused tree mortality depending on the latitude of the fire, regional assessments of trends in burn severity (Dillon et al. 2011, Harvey et al. 2016*b*, Parks et al. 2018*a*) could be challenging if they do not account for latitudinal effects. The effect on satellite indices of burn severity from more direct sun angles at lower latitudes has been discussed in the literature (French et al. 2008, Parks et al. 2014*a*), but has not been systematically tested or quantified across wide swaths of latitude. In addition, whether the relationship between satellite and field measures of burn severity is consistent across gradients of past (pre-fire) disturbances such as insect outbreaks is unknown (see McCarley et al. 2017 for an example comparing spectral measures of burn severity to LiDAR measures of burn severity), yet remote sensing is a valuable tool for measuring burn severity in beetle-impacted forests (Meigs et al. 2016). Without knowing how the reliability of satellite burn severity indices may be affected by gradients in geography, topography, and stand structure, insights into how disturbance regimes are changing are constrained in important ways.

We address the above research gaps by asking three research questions that compare satellite burn severity indices to individual field measures of burn severity across key ecological gradients in a large, fire-prone, temperate forested region. First, we asked which of three commonly used satellite indices (dNBR, RdNBR, or RBR) best corresponds directly to individual field measures of burn severity in forests spanning the U.S. Rocky Mountains (Q1). We expected that all three NBR-derived indices would perform similarly, but that RBR would overall be the best performing index, based on recent work in nearby ecoregions (Parks et al. 2014*a*). We also expected that indices would perform best for canopy measures of burn severity and worst for forest-floor measures of burn severity—given that the satellite has the most unobstructed view of the forest canopy. Second, using the highest ranked satellite index from Q1, we asked whether geospatial data that are typically readily available (e.g., latitude, elevation, slope, aspect, pre-fire NBR) could improve the correspondence between field and satellite measures of burn severity (Q2). We expected that inclusion of such data would lead to moderate improvements in model performance between field and satellite measures. Third, we asked how the best available models relating satellite to field indices of burn severity are affected by forest stand-structure variables that are not easily attainable without field data (e.g., basal area, pre-fire bark beetle outbreak severity; Q3). We expected that pre-fire stand structure would not affect the performance of relative indices (e.g., RBR and RdNBR) of burn severity (Miller and Thode 2007), but that pre-fire beetle outbreak severity could affect the performance of burn severity indices, based on insights using LiDAR (McCarley et al. 2017). Finally, we used an example fire from the geographic center of our study area to demonstrate how different spatial patterns emerge for individual field measures of burn severity and how incorporating the error in these estimates affects the observed spatial patterns of burn severity across a burned landscape.

Methods

Study area

The U.S. Rocky Mountains encompasses EPA level III ecoregions 15, 16, 17, 18, 19, 21, and 41, including parts of New Mexico, Utah, Colorado, Wyoming, Idaho, Montana, and Washington (Fig. 1). Forests in the region are conifer-dominated and vary compositionally along gradients of elevation and latitude (Peet 2000, Baker 2009). Forest elevations range from 1500 to 4300 m and generally decrease toward northern latitudes; that is, forests are at higher elevations at lower latitudes. Subalpine (high-elevation) forests are generally characterized by infrequent, high-severity wildfires, and are composed primarily

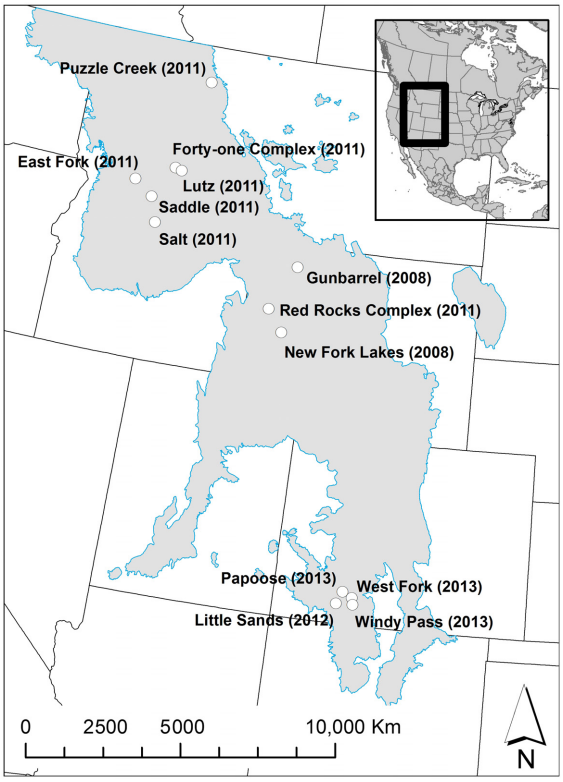

Fig. 1. Study area and sample fire locations (years in parentheses) for the 593 plots included in this study. The U.S. Rocky Mountain ecoregion is outlined in light blue and shaded in gray.

of thin-barked conifers that regenerate via seed following fire (e.g., *Pinus contorta*, *Pinus flexilis*, *Pinus albicaulis*, *Picea engelmannii*, and *Abies lasiocarpa*; Schoennagel et al. 2004, Baker 2009). Mid-montane (mid-elevation) forests are generally characterized by a mixed severity fire regime and are composed of the aforementioned thin-barked species, as well as thick-barked species that can also survive lower intensity fires (e.g., *Pinus ponderosa*, *Pseudotsuga menziesii*, *Pinus monticola*, and *Larix occidentalis*; Schoennagel et al. 2004, Baker 2009). The re-sprouting angiosperm *Populus tremuloides* rarely survives fire (but commonly colonizes burned areas) and inhabits mid-montane to lower subalpine forests. Low-montane woodlands (~500–1500 m elevation) are typified by a high-frequency but low-severity fire regime and are dominated primarily by sparse stands of *P. ponderosa*, *P. menziesii*, and *Juniperus scopulorum* (Schoennagel et al. 2004, Baker 2009).

Field measures of burn severity

We used existing field data from 496 plots in burned and unburned forest stands in 13 different fires that burned between 2008 and 2013 in representative portions of the study region (Harvey et al. 2013, 2014*a*, *b*, Andrus et al. 2016; Fig. 1; Appendix S1: Table S1). Field data covered a wide range of topographic conditions, pre-fire forest stand structure, and tree species composition that are broadly representative of the dominant forests in the Rocky Mountains (Table 1). Data from each field plot (30 m diameter circle; Harvey et al. 2013, 2014*a*, *b*; or 20×20 m^2; Andrus et al. 2016) included five individual quantitatively assessed measures of burn severity. These included three measures of canopy burn severity: percentage of tree mortality by basal area, percentage of tree mortality by number of trees, and percentage of bole circumference that was scorched; and two measures of forest-floor burn severity: char height as percentage of tree height, and percentage of charred surface cover. Char height, although measured on canopy trees, was considered a forest-floor burn severity measure as it corresponds to surface fire intensity and therefore burn severity on the forest floor. Bole scorch, however, was considered a canopy burn severity measure as it is a strong predictor of tree mortality. Complete descriptions of field methods are published elsewhere (Harvey et al. 2013, 2014*a*, *b*, Andrus et al. 2016); however, for completeness we also explain these field measures in detail in Table 2.

Covariates of geography, topography, and pre-fire stand structure

Field data on topographic setting and pre-fire forest structure were collected from each of the burned and unburned plots, following existing protocols (Harvey et al. 2013, 2014*a*, *b*, Andrus et al. 2016). In short, we recorded the elevation (m), slope (deg), aspect (azimuth), and coordinates (lat/lon, in decimal degrees) from plot center. Slope, aspect, and latitude were then used to calculate solar heat load ($MJ \cdot cm^{-1} \cdot yr^{-1}$) following published equations (McCune and Keon 2002). For each tree reaching a height of 1.4 m (and greater than 4 cm diameter; Andrus et al. 2016) in each plot, we recorded the following characteristics: live/dead (after the fire), species, diameter at breast height (dbh, to the nearest

Table 1. Descriptive statistics of physical setting, pre-fire stand structure, and pre-fire tree species composition from the 593† plots used to calibrate and validate RdNBR.

Variable	Min–max	Mean	Median
Physical setting			
Latitude (decimal deg.)	37.43–48.22	42.53	43.53
Longitude (decimal deg.)	−115.03 to −106.79	−110.12	−109.89
Elevation (m)	1735–3659	2607	2603
Slope (deg.)	1–62	19	17
Heat load ($MJ \cdot cm^{-2} \cdot yr^{-1}$)‡	0.198–1.104	0.767	0.778
Pre-fire NBR	−0.453 to 0.838	0.376	0.379
Pre-fire stand structure			
Basal area (m^2/ha)	12.9–108.2	41.5	37.7
Stand density (stems/ha)	141–5829	1506	1358
Large trees only (>10 cm dbh)	141–2122	806	850
Quadratic mean diameter, all trees (cm)	8.6–43.1	20.1	18.5
Quadratic mean diameter, trees live at fire (cm)	6.6–48.6	16.2	14.9
Maximum tree height (m)	10.0–36.0	23.8	23.4
Beetle-killed basal area (percentage of BA in stand)	0.0–99.2	35.7	30.0
Pre-fire stand composition (percentage of tree BA)			
White fir (*Abies concolor)*	0 to <1	<1	0
Grand fir (*Abies grandis*)	0–23	<1	0
Subalpine fir (*Abies lasiocarpa*)	0–88	13	3
Rocky Mountain juniper (*Juniperus scopulorum*)	0–33	<1	0
Engelmann spruce (*Picea engelmannii*)	0–100	24	0
Colorado blue spruce (*Picea pungens*)	0–74	<1	0
Whitebark pine (*Pinus albicaulis*)	0–72	2	0
Lodgepole pine (*Pinus contorta*)	0–100	35	4
Limber pine (*Pinus flexilis*)	0–72	2	0
Ponderosa pine (*Pinus ponderosa*)	0–75	<1	0
Pinus sp. (unk. beyond genus)	0–28	<1	0
Quaking aspen (*Populus tremuloides*)	0–1	<1	0
Douglas-fir (*Pseudotsuga menziesii*)	0–100	21	0
Salix sp. (unk. beyond genus)	0–5	<1	0
Unknown	0–32	1	0

† 496 field plots; 97 aerial photography plots.
‡ Calculated using formulas in McCune and Keon (2002).

0.5 cm), and if the tree was alive or dead at the time of fire (based on charring characteristics). We also recorded whether a tree had been killed by bark beetles prior to fire using established methods (Harvey et al. 2013). From the individual tree data, we calculated the following stand-structure variables for each plot: basal area (m^2/ha), stand density (stems/ha) of all trees, stand density (stems/ha) for trees >10 cm dbh, quadratic mean diameter (QMD, cm; Curtis and Marshall 2000) for all trees, QMD (cm) for trees that were alive at the time of fire, and percentage of basal area of the stand that was killed by bark beetles prior to fire.

An additional 97 unburned forest stands were added to the existing field dataset using a combination of burn severity and perimeter maps, post-fire color aerial imagery (1-m resolution from the National Agricultural Imagery Program; Aerial Photography Field Office [AFPO] 2016), and vegetation data (LandFire Environmental Site Potential; Rollins 2009). These plots were located within a 100-m external buffer from the burn perimeter and were visually assessed for any evidence of disturbance. In the unburned plots, we visually estimated canopy mortality from bark beetle outbreaks to the nearest 10% using 1-m resolution color aerial imagery; presence of bark beetle outbreaks was corroborated with U.S. Forest Service Aerial Detection Surveys (http://www.fs.fed.us/foresthealth/aviation/aerialsurvey.shtml).

Table 2. Descriptive statistics of satellite and field measures of burn severity from the 593† plots used in models.

Burn severity metric	Description	Min–max	Mean	Median
Satellite measures				
dNBR (index)	Differenced Normalized Burn Ratio (Key and Benson 2005)	−165 to 1040	365	342
RdNBR (index)	Relative differenced Normalized Burn Ratio (Miller and Thode 2007)	−370 to 2079	609	627
RBR (index	Relative Burn Ratio (Parks et al. 2014*a*)	−148 to 654	262	264
Field measures: canopy severity				
Basal area killed by fire (%)	The percentage of tree basal area per plot that was alive at the time of fire and killed by the fire	0–100	66	100
Trees killed by fire (%)	The percentage of trees per plot that were alive at the time of fire and killed by the fire	0–100	67	100
Bole scorching (percentage of circumference)	Average percent of tree bole circumference that was charred from randomly selected dominant canopy trees (20/plot) that were alive at the time of fire. This value was the maximum percentage at any height on the bole	0–100	67	89
Field measures: Forest-floor severity				
Char height (percentage of tree height)	Average percent of total tree height that was charred from randomly selected dominant canopy trees (20/plot) that were alive at the time of fire	0–100	36	27
Charred surface cover (%)	Average percent of charred ground cover in plots, taken from 480 to 500 points >10 cm apart along the main plot axis (N-S, E-W)	0–100	36	27

† 496 field plots; 97 aerial photography plots.

We summed or averaged all values to the plot level before analysis. Summary statistics of topographic and stand-structure variables across our plots are in Table 1.

Satellite measures of burn severity

We acquired satellite burn severity data (dNBR and RdNBR extended assessments) and pre- and 1-yr post-fire Landsat imagery at 30-m resolution for each of the study fires (Fig. 1; Appendix S1: Table S2) from the Monitoring Trends in Burn Severity (MTBS) database (Eidenshink et al. 2007; www.mtbs.gov). We then computed RBR (Parks et al. 2014*a*) using the pre-fire Landsat imagery, dNBR, and dNBR offset value included in the MTBS metadata to ensure all burn severity data were consistent and computed from the same base imagery, following methods in Parks et al. (2014*b*). For each of our 593 plots, we extracted the dNBR, RBR, and RdNBR value of the focal pixel and bilinear interpolated (weighted average value based on the four nearest neighbors to focal pixel) value from the burn severity data using the raster package (Hijmans et al. 2017) in the statistical software R (R Development Core Team 2018). Previous research suggests that the bilinear interpolation subsampling method performs better than other subsampling methods such as cubic convolution and nearest neighbor (Cansler and McKenzie 2012). Preliminary analysis demonstrated that values extracted from bilinear interpolation for each plot location performed consistently better than extracting the value from the focal pixel (Appendix S1: Figs. S1, S2); therefore, we performed all subsequent analyses on the bilinear interpolated values. We excluded any points with missing data in the satellite image caused by the scanner line correction failure on the Landsat 7 satellite. Values of burn severity metrics ranged from unburned with vegetation growth (dNBR: −165, RdNBR: −370, RBR: −148) to very high burn severity (dNBR: 1040, RdNBR: 2079, RBR: 654; Table 2).

Data analysis

Each of our research questions required a statistical model to predict the proportion of each burn severity field measure based on satellite burn severity metrics and other possible biophysical covariates. These proportions of field burn severity could range from zero (e.g., unburned)

to one (e.g., completely burned). Beta regression, in which a logit link is coupled with a beta distribution observation model (Ferrari and Cribari-Neto 2004), can model proportions between zero and one, but cannot account for the zeros or ones themselves. Therefore, we fit zero/one inflated beta (ZOIB) hierarchical regression models (Ospina and Ferrari 2012, Liu and Kong 2015), which allow for zeros, ones, and continuous proportions between these bounds.

Following the notation of Liu and Kong (2015), ZOIB models assume that the response data y (here, a proportion value for each burn severity metric, ranging from zero to one) for observation i follow a piecewise distribution such that

$$f(y_i) = \begin{cases} p_i & \text{if } y_i = 0, \\ (1 - p_i)q_i & \text{if } y_i = 1, \\ (1 - p_i)(1 - q_i)\text{Beta}(a_i, b_i) & \text{if } y_i \in (0, 1), \end{cases}$$

where p_i represents the probability $\Pr(y_i = 0)$, q_i represents the conditional probability $\Pr(y_i = 1 | y_i \neq 0)$, and a_i and b_i represent the beta distribution shape parameters for $y_i \in (0, 1)$. We can combine these components to derive the unconditional estimate of the response $E(y_i)$ (Liu and Kong 2015) as

$$E(y_i) = (1 - p_i)\left(q_i + (1 - q_i)\mu_i^{(0,1)}\right).$$

For datasets in which we did not have any zeros, we fit a one-inflated beta model, which is similar to the ZOIB model except it omits p_i

$$E(y_i) = q_i + (1 - q_i)\mu_i^{(0,1)}.$$

Fitting the piecewise distribution requires fitting the following component models in which we use the superscripts p, q, and r to represent related data and parameters across the three models. First, we fit a model to the zeros vs. non-zeros

$$\begin{aligned} y_i^p &\sim \text{Binomial}(p_i) \\ p_i &= \text{logit}^{-1}(\alpha^p + \alpha_{j[i]}^p + \mathbf{X}_i^p \boldsymbol{\beta}^p) \end{aligned}$$

where y_i^p is a series of zeros and ones with a one representing that the original data $y_i = 0$. The symbol $\mathbf{X}_i$ represents a vector of predictors and $\boldsymbol{\beta}$ a vector of slope coefficients. The parameter α represents an intercept, and $\alpha_{j[i]}$ represents a fire-specific intercept (indexed by j) that is allowed to vary and is constrained by a normal distribution in logit space (i.e., a "random intercept")

$$\alpha_j^p \sim \text{Normal}(0, \sigma_p^2).$$

Second, we fit a model to the ones vs. non-ones for all cases that were not $y_i = 0$, with y_i^q representing a series of ones and zeros with one representing that the original data $y_i = 1 | y_i \neq 0$

$$\begin{aligned} y_i^q &\sim \text{Binomial}(q_i) \\ q_i &= \text{logit}^{-1}\left(\alpha^q + \alpha_{j[i]}^q + \mathbf{X}_i^q \boldsymbol{\beta}^q\right) \\ \alpha_j^q &\sim \text{Normal}(0, \sigma_q^2). \end{aligned}$$

Third, we fit a model to the proportional data for all cases of y_i that were not exactly zero or one

$$\begin{aligned} y_i^r &\sim \text{Beta}(a_i, b_i) \\ a_i &= \phi\mu_i \\ b_i &= \phi(1 - \mu_i) \\ \mu_i &= \text{logit}^{-1}(\alpha^r + \alpha_{j[i]}^r + \mathbf{X}_i^r \boldsymbol{\beta}^r) \\ \alpha_j^r &\sim \text{Normal}(0, \sigma_r^2) \end{aligned}$$

where y_i^r represents a proportional value between zero and one. We rearranged the beta distribution so that the two shape parameters were represented by a dispersion parameter ϕ (controlling how spread out or dispersed the distribution will be) and a mean parameter μ_i (Ferrari and Cribari-Neto 2004).

We fit the ZOIB models with Stan (Carpenter et al. 2017) and rstan (Stan Development Team 2018) for R (R Development Core Team 2018). After standardizing the predictors by subtracting their means and dividing them by two times their standard deviations (Gelman 2008), we placed weakly informative priors of Normal(0, 5) on the intercepts α, Normal(0, 2) on the slope parameters $\boldsymbol{\beta}$, Half-t(3, 0, 25) on the dispersion parameter ϕ (i.e., a Student t distribution with degrees of freedom 3 and scale 25 for values >0), and Half-t(3, 0, 2) priors on the σ parameters. For each model, we sampled from the posterior with 1000 iterations across four chains and discarded the first half of each chain as warm-up. We ensured consistency with chain convergence by ensuring $\hat{R}$ (the potential scale reduction factor) was <1.05 and the minimum effective sample size n_{eff} was >100 for all parameters (Gelman et al. 2014).

For Q1, we fit ZOIB models testing the bivariate relationship between the satellite and field measures of burn severity. For Q2, we added the main effects of commonly available biophysical variables and their interactions with each satellite metric of burn severity. For Q3, we included stand-specific variables acquired from the field and their interactions with satellite metrics. For Q2 and Q3, our main focus of inference was on the interaction coefficients rather than the main effects. A positive interaction, for example, would indicate that as the value of the biophysical term in the model (e.g., latitude) increased, the slope between the satellite and field measures of burn severity became steeper. Since there are three components to the ZOIB model, there are three versions of each interaction, which can be visualized in aggregate by combining the component models into their combined expectation $E(y_i)$ at various values of the biophysical variables. We chose to avoid model selection and conduct inference on the full statistical models (Gelman and Rubin 1995). Since we used a Bayesian approach, and removing a variable would be equivalent to setting its prior to exactly zero, we instead used weakly informative priors and retained all predictors. However, we note that predictors with effects near or encompassing zero would make little difference to the predictions if they were omitted (e.g., if they were unavailable or costly to collect).

We evaluated model fit via the area under receiver operating curves (AUC) across a sequence of thresholds. Calculating the AUC involves dichotomizing the field response proportions into a series of ones and zeros depending on whether they are above or below a specific proportion threshold, and then calculating the probability that the model would correctly rank a randomly chosen observation now coded as a one as more burned than a less burned observation now coded as a zero. We evaluated AUC at thresholds of 0.050, 0.275, 0.500, 0.725, and 0.950. For simplicity, we performed these calculations on the median posterior predictions instead of across all samples from the posterior. We initially tried a cross-validated evaluation of model performance for Q1, where we successively left out each fire from model building and predicted the omitted data. However, we found this made little qualitative difference to the results since no one fire substantially drove the model. Therefore, we chose to present the results without cross-validation for simplicity.

Finally, to visually demonstrate differences in the relationship between satellite indices and individual field measures of burn severity, uncertainty in estimates of those relationships, and the collective effect on interpreting burn severity patterns, we used the best models from Q1 (without geospatial covariates) and Q2 (with geospatial covariates) to produce maps of tree mortality and charred surface cover (and 90% quantile credible intervals for each estimate) for a fire nearest the geographic center of our study area. We did not extrapolate predictions beyond the range of RdNBR upon which we built a model, and all RdNBR values less than −500 and greater than 2500 were excluded from analyses.

Results

Overall, dNBR, RdNBR, and RBR performed similarly in bivariate comparisons with field measures of burn severity, but some minor differences emerged for certain field measures and at different levels of burn severity in the field (Fig. 2). Area under receiver operating curves (AUC) values of satellite correspondence to field burn severity were generally high and indicated strong model performance (ranging from ~0.80 to ~0.95) across all satellite and field measures (Fig. 2a–e). However, model performance was consistently higher for canopy measures of burn severity (tree mortality and bole scorch, Fig. 2a–c) and consistently lower for forest-floor measures of burn severity (char height and charred surface cover, Fig. 2d–e). Area under receiver operating curves (AUC) decreased with increasing burn severity for all satellite indices and field measures (Fig. 2a–e; Appendix S1: Fig. S3); decreases in AUC with increasing burn severity were most pronounced for forest-floor measures of burn severity (Fig. 2d, e) and subtler for canopy measures of burn severity (Fig. 2a–c). Similarities in performance among satellite indices were strongest at low levels of burn severity, whereas performance diverged at higher burn severity. Where indices diverged at higher burn severity, RdNBR was most often the model with the best performance (highest AUC)

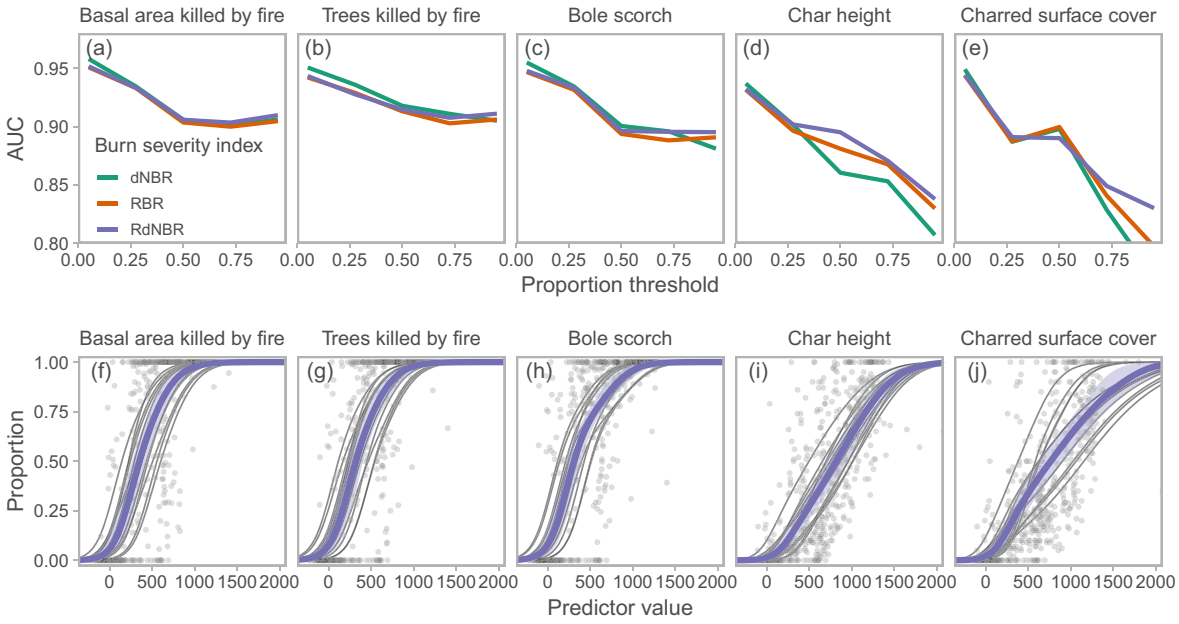

Fig. 2. Bivariate models comparing each field measure of burn severity (5 measures, left to right) to each satellite index of burn severity (solid lines: green = dNBR; orange = RBR; purple = RdNBR). (a–e) Median global posterior (purple) and 95% credible intervals (shaded) along with fire-specific random-effect median posteriors shown as gray lines for the RdNBR ZOIB model. Raw data are shown as dots. (f–j) Model performance was evaluated by comparing AUC values along the gradient of each field burn severity metric (left, less severe, to right, more severe, on the *x*-axis). Higher AUC values correspond to stronger model predictive performance and represent the probability that the model would correctly rank a randomly chosen observation that is above the threshold as more burned than a less burned observation that is below the threshold. AUC, area under receiver operating curves; dNBR, differenced normalized burn ratio; RBR, relative burn ratio; RdNBR, relative differenced normalized burn ratio; ZOIB, zero/one inflated beta.

and RBR and dNBR were slightly poorer (Fig. 2a–e; Appendix S1: Fig. S2). Because RdNBR was overall the best performing satellite index, and for simplicity, results hereafter (for Q2 and Q3) are presented for RdNBR only (Fig. 2f–j).

Each of the geospatial variables affected the relationship between field measures of burn severity and RdNBR, but to varying degrees (Fig. 3). Latitude and pre-fire NBR had the strongest effect on the relationship between RdNBR and field measures (Fig. 3f–o). More northerly latitudes led to a steeper slope between RdNBR and canopy burn severity (Fig. 3f–h); however, latitude had the opposite effect on the relationship between RdNBR and forest-floor burn severity (Fig. 3i, j); that is, the same value of RdNBR corresponded to greater canopy burn severity at more northerly latitudes, but to lower forest-floor burn severity at more northerly latitudes. Higher values of pre-fire NBR consistently led to a steeper slope between RdNBR and all field measures of burn severity, meaning that the same value of RdNBR corresponded to greater burn severity in the field at higher levels of pre-fire NBR (Fig. 3k–o). This effect was strongest for bole scorch, char height, and charred surface cover (Fig. 3m–o), weakest for both measures of tree mortality (Fig. 3k, l) and was accentuated at mid to high levels of RdNBR. Topographic variables—heat load index (Fig. 3a–e) and slope (Fig. 3p–t)—had minor effects on the relationship between RdNBR and field measures of burn severity. The most notable difference was the effect of heat load index, such that the same value of RdNBR corresponds to lower

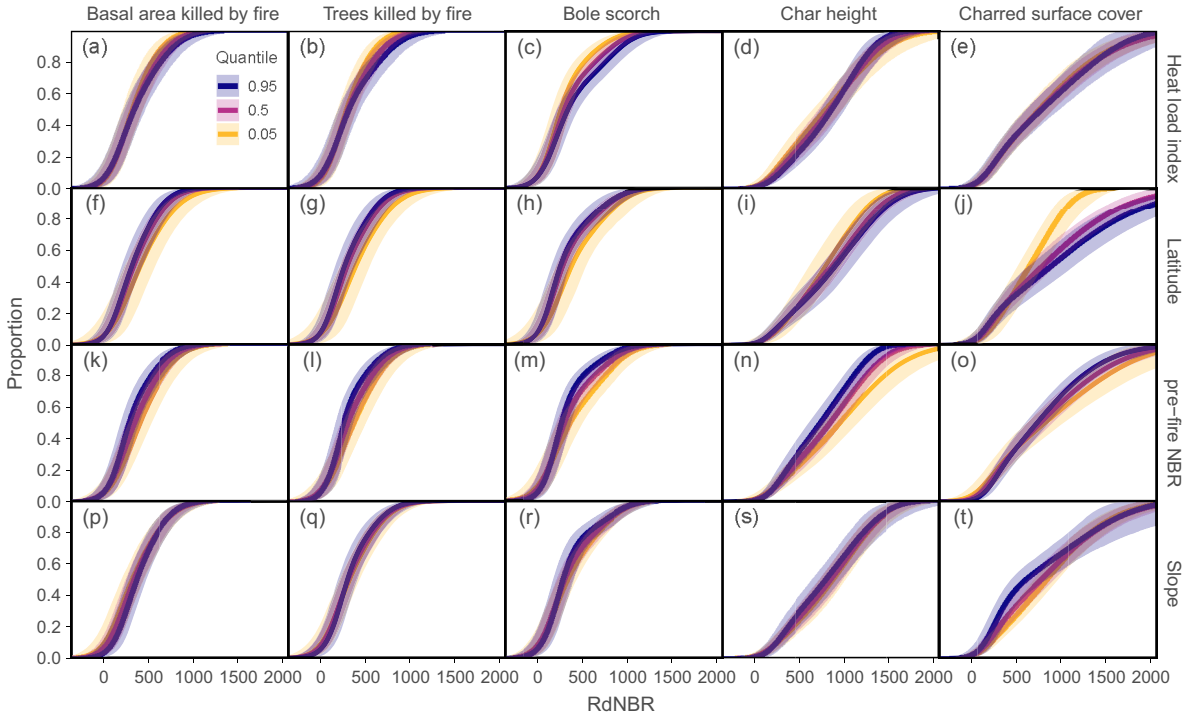

Fig. 3. Change in relationship between relative differenced normalized burn ratio (RdNBR; *x*-axis) and field measures of burn severity (*y*-axis, different field measures in columns from left to right) across gradients of Heat Load Index (row 1), latitude (row 2), pre-fire normalized burn ratio (row 3), and slope (row 4). Colored lines represent modeled relationship at the 5th (yellow), 50th (purple), and 95th (blue) percentiles of the gradient of interest (rows, labels on right *y*-axis). Solid lines represent posterior medians, and shaded regions represent 90% credible intervals.

canopy burn severity (bole scorch and trees killed by fire, Fig. 3a–c) in areas with higher heat load index. Standardized model coefficients for interaction terms of each variable with RdNBR varied in size, but were generally largest for latitude and pre-fire NBR (Fig. 4).

When complementing RdNBR models of burn severity with geospatial variables, model improvement was consistent across nearly all field measures of burn severity, raising AUC values by ~0.02 across levels of burn severity (Fig. 5). The same general pattern as the bivariate models (Fig. 2) was evident, in that AUC was generally highest at lower levels of burn severity, and that models performed better for measures of canopy burn severity (Fig. 5a–c) than for forest-floor burn severity (Fig. 5d–e). The highest improvement was for charred surface cover (Fig. 5e), in which AUC improved by over 0.1 probability units at high levels of burn severity, and the lowest improvement was for char height (Fig. 5d).

Most forest stand-structure variables affected the relationship between field measures of burn severity and RdNBR (Fig. 6). The strongest effects were from pre-fire beetle outbreak severity (Fig. 6a–e), QMD (Fig. 6f–j), and basal area (Fig. 6k–o); stand density had weaker effects on the performance of RdNBR (Fig. 6p–t). In some cases, the position of the slope representing the relationship between field measures of burn severity and RdNBR was shifted; that is, slopes did not substantively differ, but they were offset. For example, the effect of QMD on canopy burn severity was to shift the lines along the *x*-axis, such that the same level of RdNBR nearly always corresponded to greater canopy burn severity in the field at higher levels of pre-fire QMD (Fig. 6f–h). In other cases, the actual slopes of the relationship between field measures of burn

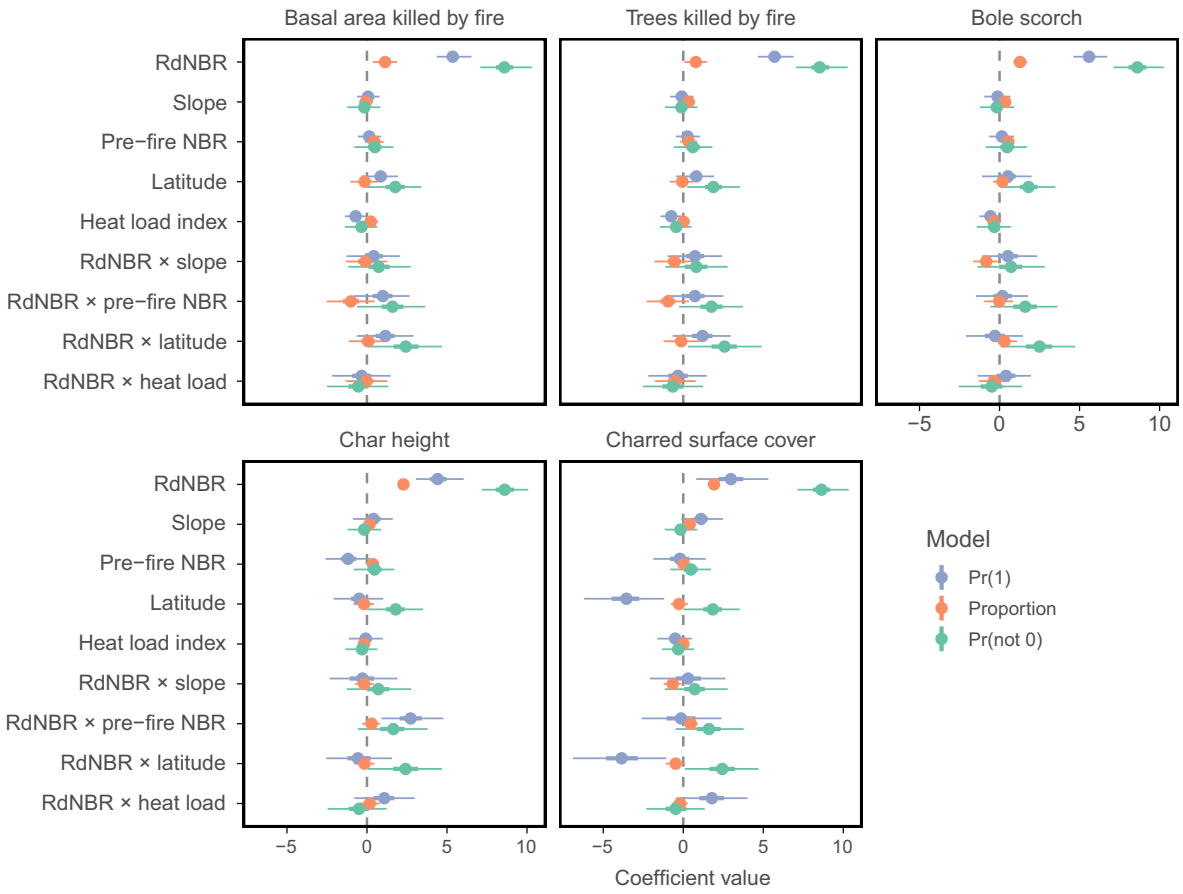

Fig. 4. Coefficient plots illustrating the effect of geospatial variables on the relationship between relative differenced normalized burn ratio (RdNBR) and field measures of burn severity. Dots represent the medians of the posteriors, and horizontal lines represent 95% and 50% credible intervals (thin and thick lines). The effects are per 2 standard deviations for each predictor and in log-odd units (i.e., in logit space). Green represents the effect of each term on the probability of being not being completely unburned, red/orange represents the effect of each term on the proportion of severity (between 0 and 1), and blue/purple represents the effect of each term on the probability of burning at highest severity (if not unburned). Interaction terms are the focus of this analysis: The stronger the interaction term between each variable and RdNBR, the stronger the effect of that variable on the relationship between RdNBR and burn severity measured in the field.

severity and RdNBR changed across the spectrum of stand structure. For example, in areas with high QMD, charred surface cover was greater than expected at low levels of RdNBR and lower than expected at high levels of RdNBR (Fig. 6j). Pre-fire beetle outbreak severity and pre-fire basal area had similar effects on the relationship between RdNBR and canopy burn severity. In general, greater pre-fire beetle outbreak severity and greater pre-fire basal area resulted in higher than expected levels of canopy burn severity at lower RdNBR and in lower than expected levels of canopy burn severity at higher RdNBR (Fig. 6a–c, k–m). Standardized model coefficients for interaction terms of each stand-structure variable with RdNBR varied in size, the strongest support for interaction terms was for pre-fire beetle outbreak severity and basal area on the relationship between RdNBR and measures of canopy burn severity (Fig. 7).

Accounting for the shape of the relationship between RdNBR and individually distinct field

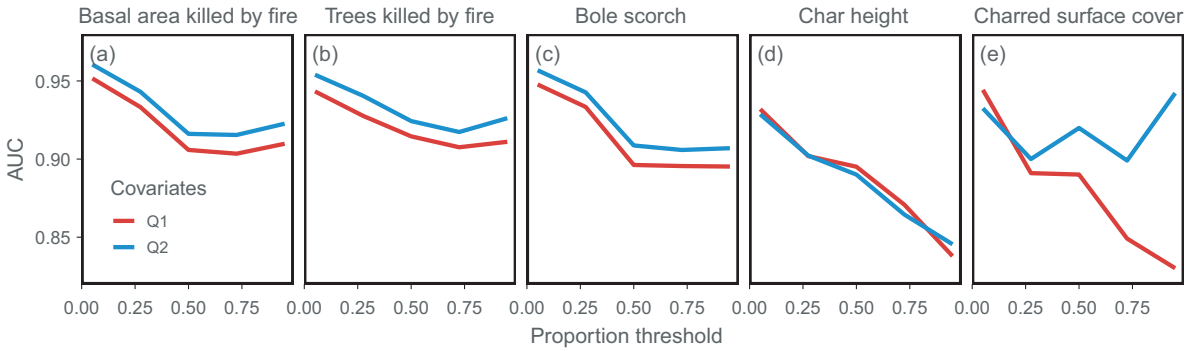

Fig. 5. Comparison of raw bivariate models (red line) between each field measure of burn severity (5 measures, left to right) with relative differenced normalized burn ratio (Q1) vs. full models that include geospatial variables (Q2) that can affect relationships between field and satellite measures of burn severity (blue line). Model performance was evaluated by comparing area under receiver operating curves (AUC) values along the gradient of each field burn severity metric (left, less severe, to right, more severe, on the *x*-axis). Greater AUC values correspond to stronger model predictive performance.

measures of burn severity, error in those relationships, and the effects of geospatial variables in Q2 produces substantively different maps of burn severity for a single fire (Fig. 8; Appendix S1: Fig. S4). When using the median model predictions, burn severity among individual components differed qualitatively in their spatial patterns; in this case, tree mortality (Fig. 8d) was more severe across the fire than forest-floor burn severity (Fig. 8e). Incorporating modeled observation error between field and satellite measures of burn severity also demonstrates wide differences in spatial burn severity patterns within individual components of burn severity. Spatial patterns of burn severity differed widely between the lower and upper bounds of the 90% credible intervals for both forest-floor burn severity (Fig. 8b, f) and canopy burn severity (Fig. 8c, g). Accounting for the effects of geospatial variables on the relationship between satellite indices and field measures of burn severity resulted in pixel-level differences in burn severity estimates ranging from −20% to +20% of the predicted values compared to when geospatial covariates were not considered (Fig. 8h–i).

Discussion

Accurately detecting the ecological severity of forest fires over broad regions is critical to characterizing, monitoring, and analyzing disturbance regimes, and it is of paramount importance in a warmer and more fire-prone climate as disturbance regimes are changing. By testing the performance of three commonly used satellite burn severity indices against individual field measures of canopy and forest-floor burn severity across biophysical gradients, our study makes several important contributions to the continued use of satellite indices in tracking burn severity in forests. First, there were minor differences in performance among NBR-derived indices, though RdNBR performed better overall than dNBR or RBR. Second, geographic, topographic, and pre-fire reflectance information improved model fit for the best performing index (RdNBR), and since these geospatial data are readily and freely available in geographic information systems (GIS) format, inclusion of such information should lead to improved accuracy in burn severity mapping. Third, the relationship between satellite and field measures of burn severity was also affected by stand-structure variables that are typically only available via detailed field data. As such, the use of satellite indices should be cautioned across wide gradients of stand structure (e.g., tree basal area or average tree size) and pre-fire disturbances (e.g., bark beetle outbreaks)—unless accurate data for these variables are available and used to calibrate satellite burn severity indices. Fourth, the above differences in the relationship among satellite

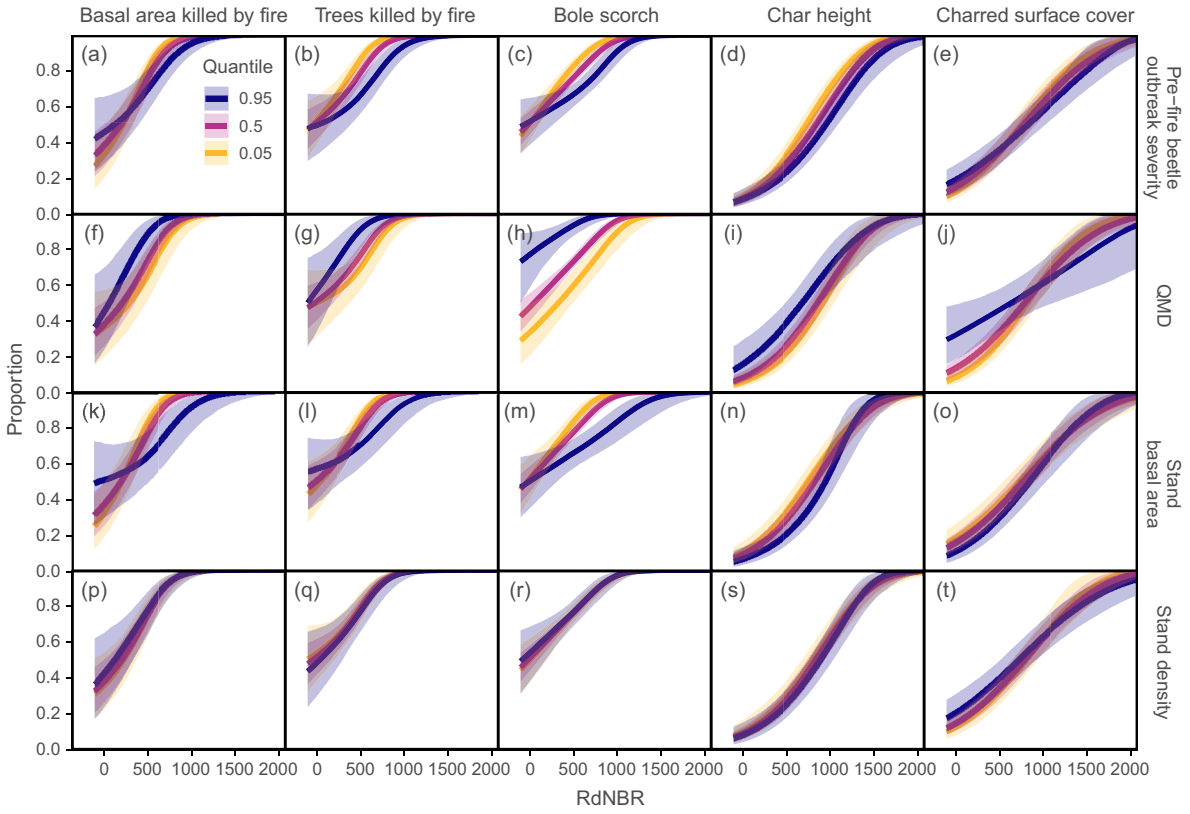

Fig. 6. Change in relationship between relative differenced normalized burn ratio (RdNBR; *x*-axis) and field measures of burn severity (*y*-axis, different measures in columns from left to right) across gradients of pre-fire beetle outbreak severity (row 1), quadratic mean diameter (QMD; row 2), basal area per ha (row 3), and stems per ha (row 4). Colored lines represent modeled relationship at the 5th (yellow), 50th (red), and 95th (blue) percentiles of the gradient of interest (rows, labels on right *y*-axis). Solid lines represent posterior medians, and shaded regions represent 90% credible intervals.

indices and individual components of burn severity in the field, as well as the error in estimating those relationships, can have important impacts on mapping burn severity. Below, we expand on each of these points and discuss future directions that could build from this study.

Overall, we found that of the three satellite indices of burn severity that we tested, RdNBR performed best. Differences among RdNBR and other indices were particularly strong at the highest levels of burn severity, where performance diverged among all three indices. Our prediction that RBR would be the best performing index of burn severity was not supported; however, differences among indices were subtle. Similar performance among indices likely results from the fact that all three indices are slightly different derivatives of the normalized burn ratio (Key and Benson 2005); that is, they are all starting with the same information from Landsat bands that measure reflectance in near-infrared and shortwave-infrared wavelengths. Past comparisons between RdNBR and dNBR have also found minor quantitative differences in performance between indices (Miller and Thode 2007, Cansler and McKenzie 2012), as have comparisons that also include RBR (Parks et al. 2014*a*, 2018*b*, Whitman et al. 2018). Our findings support the idea that relative indices (e.g., RdNBR and RBR) fit better to field data than absolute indices (e.g., dNBR), as has been reported elsewhere (Miller and Thode 2007, Parks et al. 2014*a*, Whitman et al. 2018) and that canopy measures of burn severity are captured more accurately

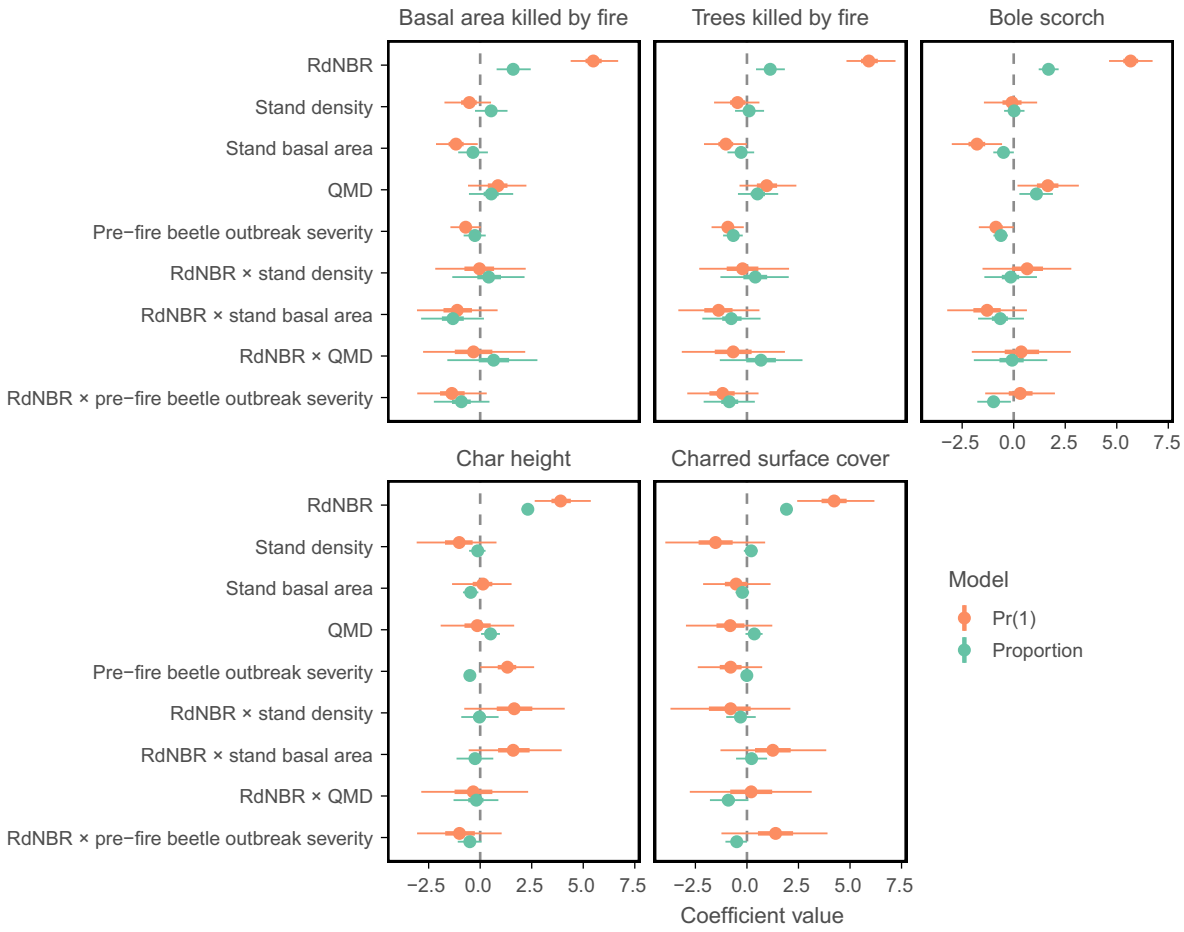

Fig. 7. Coefficient plots illustrating the effect of stand-structure variables and pre-fire beetle outbreak severity on the relationship between relative differenced normalized burn ratio (RdNBR) and field measures of burn severity. The legend is otherwise the same as for Fig. 4 except that there is no Pr(0) model since there were not cases that were completely unburned that had all of these covariates.

than forest-floor measures (Hudak et al. 2007). Given the current focus in many regions on trends in high-severity (i.e., stand-replacing or canopy-removing) fire (Miller et al. 2012, Harvey et al. 2016*b*, Stevens et al. 2017, Parks et al. 2018*a*), our results suggest that RdNBR may be the most useful satellite index among the three we tested, as the biggest differences between performance of RdNBR and other indices were at the high end of the burn severity gradient (Fig. 2a–e).

Our finding that RdNBR was affected by geospatial variables suggests that accuracy in satellite-based burn severity maps can be improved by including these variables in models to improve estimates of individual fire effects onto burned landscapes. That RdNBR was affected by these biophysical variables was surprising, as RdNBR was designed to perform consistently across such gradients (Miller and Thode 2007). However, our approach of focusing on the interaction term in models to directly test the effect of biophysical variables on the relationship (rather than testing the effect of biophysical variables on burn severity sensu; Birch et al. 2015, Kane et al. 2015, Harvey et al. 2016*b*) quantifies effects that have been alluded to elsewhere. For example, the effect of the more direct sun angle at lower latitudes on the performance of satellite burn severity indices has been posited (French

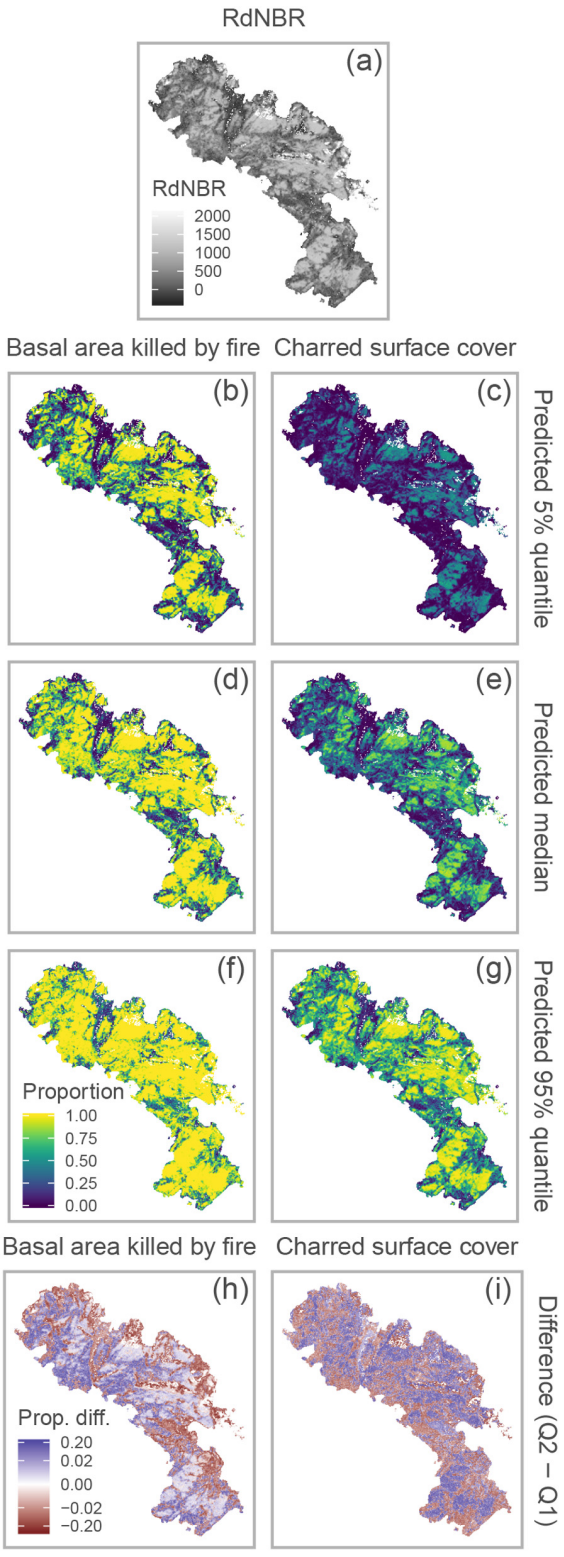

Fig. 8. Burn severity maps for the 2011 Red Rocks Fire in Wyoming, USA. (a) Map of relative differenced normalized burn ratio (RdNBR) for the region. (b–g) Maps of predicted basal area killed by fire and charred surface cover from RdNBR and interactions with geospatial variables predictors (Q2). Shown are the median, 5%, and 95% quantiles of the posterior including the beta-distributed observation model component (posterior predictions). The predictions are at the specific intercept level estimated for the Red Rocks Fire. (h, i) Difference in predicted (median) proportion of basal area killed or charred surface cover between the Q2 maps (d, e) and maps generated with only RdNBR as a predictor (Q1).

et al. 2008, Parks et al. 2014*b*), and our study provides quantitative support for this effect. Our results demonstrate that at lower latitudes (i.e., more direct sun angle) the slope of relationship between RdNBR and forest-floor burn severity steepens, possibly because at lower latitudes the forest floor receives more direct sunlight in gaps between tree crowns and there is less area within a pixel that is occupied by shadows cast from trees. This may be responsible for the corresponding shallowing of the slope in the relationship between RdNBR and canopy measures at low latitudes, as there is more top-down light interception by the crowns, whereas at higher latitudes more light is intercepted throughout the whole vertical profile of tree crowns and larger shadows are cast from trees.

Relative indices such as RdNBR were designed to decrease or eliminate the effect of pre-fire NBR on the relationship between satellite indices and field measures of burn severity (Miller and Thode 2007), but our analyses illustrate residual effects of pre-fire NBR that need to be accounted for to further improve correspondence of RdNBR to field data. As pre-fire NBR is a proxy for pre-fire biomass or canopy cover (Miller and Thode 2007), our results suggest that areas with high biomass were characterized by relationships with steeper slopes for all our models; that is, the same level of RdNBR equates to greater burn severity in areas with higher pre-fire vegetation cover—perhaps indicating that RdNBR may slightly over correct for the effect of pre-fire biomass or vegetation cover (Miller and Thode 2007). Our continuous data on stand structure

for our field plots were chosen over assigning categorical forest type variables to each plot; however, future analyses could examine how pre-fire NBR varies among forest types and therefore how this affect corresponds to categorically defined forest types.

Topographic effects on the relationship between RdNBR and field measures of burn severity were more muted than were effects of latitude and pre-fire NBR, and RdNBR appears to be more robust to variations in topography. However, the topographic effects we detected are logically consistent with the effects produced by latitude. For example, the coefficients for heat load index are inversely related to the coefficients for latitude, whereas the coefficients for slope mostly mirror those for latitude (Fig. 4). Since higher values of heat load index and lower values of latitude and slope generally correspond to greater direct solar radiation, these topographic affects could be related to the increase in long shadows cast by trees at higher latitudes and in more shaded topographic positions. For the minor effects of topography, and the more substantive effects of latitude and pre-fire NBR, geospatial data on topography and geographic location (and pre-fire NBR data which comes with the burn severity bundle downloaded from MTBS) can be applied to models that use RdNBR to map individual effects of burn severity. We suggest that doing so could result in more accurate maps of burn severity.

Relative indices of burn severity (e.g., RdNBR and RBR) are intended to improve consistency of burn severity mapping across wide ranges of pre-fire vegetation structure, but our finding that stand-structure variables (which are typically acquired through intensive field data) can affect the relationship between field and satellite measures of burn severity suggests several important points for interpreting burn severity maps. First, we suggest that caution should be taken when satellite indices are used to assess burn severity in areas affected by pre-fire beetle outbreaks (Prichard and Kennedy 2014, Meigs et al. 2016). Specifically, our findings demonstrate that the same value of RdNBR in an area affected by severe pre-fire beetle outbreaks generally corresponds to lower burn severity in the field than the same value of RdNBR in areas unaffected by beetle outbreaks prior to the fire. This suggests that, at least for the five field measures of burn severity that we included in our study, the effects of pre-fire beetle outbreak severity on subsequent burn severity may be more negative in sign than has been interpreted (Prichard and Kennedy 2014, Meigs et al. 2016). Pre-fire beetle outbreaks, where they occurred in our plots, were 1–10 yr prior to fire and in areas where most of the beetle-killed trees were still standing at the time of fire; small diameter and non-host trees comprised the live trees (Harvey et al. 2013, 2014*a*, *b*, Andrus et al. 2016). Whether longer intervals between beetle outbreaks and subsequent fire would affect the relationship between field measures and satellite indices of burn severity remains to be tested. We also found that pre-fire stand structure had important effects on the relationship between satellite indices and field measures of burn severity. The effect of pre-fire basal area on decreasing the slope between RdNBR and field measures of burn severity demonstrates, similar to the effects of pre-fire NBR above, that RdNBR may over correct for pre-fire biomass. Higher values of QMD generally correspond to stands characterized by large trees, open forests, and woodlands (e.g., ponderosa pine and Douglas-fir woodlands). In such stands, RdNBR may be less sensitive to tree mortality because of gaps between tree crowns, and therefore, lower levels of RdNBR actually correspond to higher levels of burn severity than they would in more dense forests.

Distinct relationships between satellite indices and each individual field measures of burn severity can result in widely contrasting spatial patterns of burn severity produced from the same satellite-index map, and incorporating the error in field–satellite relationships drives further variability in mapped burn severity patterns. Similar to findings in Whitman et al. (2018), we found that, when comparing individual measures of burn severity within the same fire, tree mortality burn severity was consistently greater than forest-floor burn severity, and each exhibited distinct landscape patterns (Fig. 8d–e). However, we further demonstrate that accounting for the error in satellite-derived estimates of field burn severity can drive nearly as much variability in landscape patterns of burn severity as can different individual components of burn severity (Fig. 8b–g). Future work could further test these effects by quantitatively comparing

landscape metrics of burn severity (as in Harvey et al. 2016*a*) among fires mapped using different levels of credible intervals in each burn severity metric (e.g., comparing maps representing 95th percentile estimates of burn severity to maps representing 5th percentiles).

Future research can build on the insights and limitations from this study by improving the performance of satellite imagery and mapping individual components of burn severity. First, the fact that all three of the NBR-based indices were similar in performance and continue to explain up to approximately 60–70% of the variance in field measures of burn severity (Cansler and McKenzie 2012, Parks et al. 2014*a*) indicates that further explanatory power may not be attainable using the NBR equation (Roy et al. 2006) or with analyses that are constrained by the 30-m pixel scale of Landsat imagery (Woodcock and Strahler 1987). The use of NBR-derived indices in combination with other spectral information such as spectral mixture analysis (Smith et al. 2007, 2010) may improve accuracy of burn severity maps. One particular utility of such sub-pixel approaches is separating out the fraction of shadows in each 30-m pixel, which may provide additional improvements to address the effects of latitude. Combining spectral mixture analyses with incorporation of variables that we show to affect the relationship between NBR-based indices and field measures of burn severity may hold promise in future analyses. Second, all field plots in our study were located in mature forests that had not experienced recent (e.g., within the last 30 yr) fires; therefore, canopy trees were generally ~20 m tall and several centuries old at the time of fire. However, forests that have burned severely and more than once in the last several decades may be characterized by small-statured vegetation (e.g., tree seedlings, shrubs, herbs) at the time of the second fire (Coop et al. 2016). Therefore, inquiries into the severity of short-succession re-burns (Parks et al. 2014*b*, Harvey et al. 2016*a*) could benefit from additional studies that use our approach to compare satellite indices to field measurements of burn severity in younger burned forests. Third, the lack of pre-fire field data in our study was a limitation common to many studies examining fire effects. While the use of our direct quantitative measures of burn severity in the field provides information that has more dimensions that a single CBI value, quantitative pre- and post-fire field measurements could improve opportunities to test the relationship between RdNBR and other components of fine-fuel (e.g., needles, litter, and duff) consumption that are difficult to measure post-fire. Finally, regional studies and meta-analyses are needed to test the relationship between RdNBR and individual field measures of burn severity within and among locations (Morgan et al. 2014, Kolden et al. 2015). In plots where individual field measures of burn severity are collected along with CBI data, such studies could also include analyses to cross-walk values of CBI with the direct measures of burn severity we report here.

Conclusions

Accurately tracking burn severity across space and time is critical during an era when fire regimes are rapidly shifting. Our findings demonstrate that relationships between satellite indices and individual field measures of burn severity vary considerably among canopy and forest-floor measures of burn severity, and are affected by several biophysical variables. As some of these biophysical variables are easily acquired with existing geospatial data (e.g., latitude, pre-fire NBR), incorporation of those data can improve accuracy of mapping actual burn severity on the ground in regions where these data are used to calibrate satellite burn severity indices. However, unless similar geospatial data exist for forest stand-structure variables (e.g., basal area and pre-fire beetle outbreaks) we suggest caution when interpreting burn severity from satellite indices in regions with wide gradients in these variables, as they affected the accuracy of RdNBR for mapping burn severity. Finally, we demonstrate the importance of incorporating uncertainty in burn severity maps when examining landscape patterns of burn severity—as such landscape patterns vary widely from error in estimates alone. Our results are from the U.S. Rocky Mountains; however, the approaches we employed can be applied elsewhere, and by quantitatively capturing distinct components of burn severity with individual models, burn severity can be characterized and mapped for unique components of a forest.

Acknowledgments

We thank M. Turner, D. Donato, and W. Romme for stimulating discussions leading to the conception of this study, and A. Edward and three anonymous reviewers who provided constructive comments on earlier submitted versions of this manuscript. B. Weiland, T. Butusov. N. LaBonte, S. Armstrong, A. Meiritz, Z. Osterholz, D. Guerrero-Harvey, C. Harvey, M. Harvey, D. Donato, C. Bordner, S. Fiske, and C.J. Cornell helped with fieldwork. S. Kochaver, K. Burkhard, S. Winter, K. Budke, A. Singh, and P. Townsend helped with data processing and initial models of satellite vs. field measures of burn severity. Data used in this study were funded by a Graduate Research Innovation Award from the U.S. Joint Fire Science Program (award # 12-3-01-3), the U.S. National Park Service—George Melendez Wright Climate Change Fellowship, the Laurel Salton Clark Memorial Research Fellowship from the Wisconsin Space Grant Consortium, and a David H. Smith Research Fellowship awarded to BJH; and by the National Science Foundation award 1262687. All code and data associated with this paper are available https://doi.org/10.5281/zenodo.2557846.

Literature Cited

Abatzoglou, J. T., and A. P. Williams. 2016. Impact of anthropogenic climate change on wildfire across western US forests. Proceedings of the National Academy of Sciences USA 113:11770–11775.

Aerial Photography Field Office (AFPO). 2016. Imagery programs: National Agriculture Imagery Program (NAIP). https://www.fsa.usda.gov/programs-and-services/aerial-photography/imagery-programs/naip-imagery/index

Agee, J. K. 1996. Fire ecology of Pacific Northwest Forests. Second edition. Island Press, Seattle, Washington, USA.

Andrus, R. A., T. T. Veblen, B. J. Harvey, and S. J. Hart. 2016. Fire severity unaffected by spruce beetle outbreak in spruce-fir forests in southwestern Colorado. Ecological Applications 26:700–711.

Attiwill, P. M. 1994. Ecological disturbance and the conservative management of eucalypt forests in Australia. Forest Ecology and Management 63:301–346.

Baker, W. L. 2009. Fire ecology in Rocky Mountain landscapes. Island Press, Washington, D.C., USA.

Birch, D. S., P. Morgan, C. A. Kolden, J. T. Abatzoglou, G. K. Dillon, A. T. Hudak, and A. M. S. Smith. 2015. Vegetation, topography and daily weather influenced burn severity in central Idaho and western Montana forests. Ecosphere 6:art17.

Cansler, C. A., and D. McKenzie. 2012. How robust are burn severity indices when applied in a new region? Evaluation of alternate field-based and remote-sensing methods. Remote Sensing 4:456–483.

Cansler, C. A., and D. McKenzie. 2014. Climate, fire size, and biophysical setting control fire severity and spatial pattern in the northern Cascade Range, USA. Ecological Applications 24:1037–1056.

Carpenter, B., A. Gelman, M. D. Hoffman, D. Lee, B. Goodrich, M. Betancourt, M. Brubaker, J. Guo, P. Li, and A. Riddell. 2017. Stan: A probabilistic programming language. Journal of Statistical Software 76:1–32.

Cocke, A. E., P. Z. Fulé, and J. E. Crouse. 2005. Comparison of burn severity assessments using differenced normalized burn ratio and ground data. International Journal of Wildland Fire 14:189–198.

Coop, J. D., S. A. Parks, S. R. McClernan, and L. M. Holsinger. 2016. Influences of prior wildfires on vegetation response to subsequent fire in a reburned Southwestern landscape. Ecological Applications 26:346–354.

Curtis, R. O., and D. D. Marshall. 2000. Why quadratic mean diameter? Western Journal of Applied Forestry 15:137–139.

De Santis, A., and E. Chuvieco. 2007. Burn severity estimation from remotely sensed data: performance of simulation versus empirical models. Remote Sensing of Environment 108:422–435.

Dillon, G. K., Z. A. Holden, P. Morgan, M. A. Crimmins, E. K. Heyerdahl, and C. H. Luce. 2011. Both topography and climate affected forest and woodland burn severity in two regions of the western US, 1984 to 2006. Ecosphere 2:art130.

Eidenshink, J., B. Schwind, K. Brewer, Z.-L. Zhu, B. Quayle, and S. Howard. 2007. A project for monitoring trends in burn severity. Fire Ecology 3:3–21.

Ferrari, S., and F. Cribari-Neto. 2004. Beta regression for modelling rates and proportions. Journal of Applied Statistics 31:799–815.

Flannigan, M., A. S. Cantin, W. J. de Groot, M. Wotton, A. Newbery, and L. M. Gowman. 2013. Global wildland fire season severity in the 21st century. Forest Ecology and Management 294:54–61.

French, N. H. F., E. S. Kasischke, R. J. Hall, K. A. Murphy, D. L. Verbyla, E. E. Hoy, and J. L. Allen. 2008. Using Landsat data to assess fire and burn severity in the North American boreal forest region: an overview and summary of results. International Journal of Wildland Fire 17:443–462.

Gelman, A. 2008. Scaling regression inputs by dividing by two standard deviations. Statistics in Medicine 27:2865–2873.

Gelman, A., J. B. Carlin, H. S. Stern, D. B. Dunson, A. Vehtari, and D. B. Rubin. 2014. Bayesian data analysis. Third edition. Chapman and Hall/CRC, Boca Raton, Florida, USA.

Gelman, A., and D. B. Rubin. 1995. Avoiding model selection in Bayesian social research. Sociological Methodology 25:165–173.

Harvey, B. J., D. C. Donato, W. H. Romme, and M. G. Turner. 2013. Influence of recent bark beetle outbreak on fire severity and postfire tree regeneration in montane Douglas-fir forests. Ecology 94:2475–2486.

Harvey, B. J., D. C. Donato, W. H. Romme, and M. G. Turner. 2014*a*. Fire severity and tree regeneration following bark beetle outbreaks: the role of outbreak stage and burning conditions. Ecological Applications 24:1608–1625.

Harvey, B. J., D. C. Donato, and M. G. Turner. 2014*b*. Recent mountain pine beetle outbreaks, wildfire severity, and postfire tree regeneration in the US Northern Rockies. Proceedings of the National Academy of Sciences USA 111:15120–15125.

Harvey, B. J., D. C. Donato, and M. G. Turner. 2016*a*. Burn me twice, shame on who? Interactions between successive forest fires across a temperate mountain region. Ecology 97:2272–2282.

Harvey, B. J., D. C. Donato, and M. G. Turner. 2016*b*. Drivers and trends in landscape patterns of stand-replacing fire in forests of the US Northern Rocky Mountains (1984–2010). Landscape Ecology 31: 2367–2383.

Hijmans, R. J., et al. 2017. raster: geographic data analysis and modeling. https://cran.r-project.org/package=raster

Hudak, A. T., P. Morgan, M. J. Bobbitt, A. M. Smith, S. A. Lewis, L. B. Lentile, P. R. Robichaud, J. T. Clark, and R. A. McKinley. 2007. The relationship of multispectral satellite imagery to immediate fire effects. Fire Ecology 3:64–90.

Johnstone, J. F., et al. 2016. Changing disturbance regimes, ecological memory, and forest resilience. Frontiers in Ecology and the Environment 14:369–378.

Kane, V. R., C. A. Cansler, N. A. Povak, J. T. Kane, R. J. McGaughey, J. A. Lutz, D. J. Churchill, and M. P. North. 2015. Mixed severity fire effects within the Rim fire: relative importance of local climate, fire weather, topography, and forest structure. Forest Ecology and Management 358:62–79.

Keeley, J. E. 2009. Fire intensity, fire severity and burn severity: a brief review and suggested usage. International Journal of Wildland Fire 18:116.

Key, C. H., and N. C. Benson. 2005. Landscape assessment: ground measure of severity, the Composite Burn Index. *In* D. C. Lutes, editor. FIREMON: Fire effects monitoring and inventory system. USDA Forest Service, Rocky Mountain Research Station, Ogden, Utah, USA.

Kolden, C. A., A. M. S. Smith, and J. T. Abatzoglou. 2015. Limitations and utilisation of Monitoring Trends in Burn Severity products for assessing wildfire severity in the USA. International Journal of Wildland Fire 24:1023–1028.

Lentile, L. B., Z. A. Holden, A. M. S. Smith, M. J. Falkowski, A. T. Hudak, P. Morgan, S. A. Lewis, P. E. Gessler, and N. C. Benson. 2006*a*. Remote sensing techniques to assess active fire characteristics and post-fire effects. International Journal of Wildland Fire 15:319.

Lentile, L. B., F. W. Smith, and W. D. Shepperd. 2006*b*. Influence of topography and forest structure on patterns of mixed severity fire in ponderosa pine forests of the South Dakota Black Hills, USA. International Journal of Wildland Fire 15:557–566.

Lentile, L. B., P. Morgan, A. T. Hudak, M. J. Bobbitt, S. A. Lewis, A. Smith, and P. Robichaud. 2007. Post-fire burn severity and vegetation response following eight large wildfires across the western United States. Fire Ecology 3:91–108.

Lentile, L. B., F. W. Smith, and W. D. Shepperd. 2005. Patch structure, fire-scar formation, and tree regeneration in a large mixed-severity fire in the South Dakota Black Hills, USA. Canadian Journal of Forest Research 35:2875–2885.

Liu, F., and Y. Kong. 2015. zoib: An R package for Bayesian inference for beta regression and zero/one inflated beta regression. R Journal 7:34–51.

McCarley, T. R., C. A. Kolden, N. M. Vaillant, A. T. Hudak, A. M. S. Smith, B. M. Wing, B. S. Kellogg, and J. Kreitler. 2017. Multi-temporal LiDAR and Landsat quantification of fire-induced changes to forest structure. Remote Sensing of Environment 191:419–432.

McCune, B., and D. Keon. 2002. Equations for potential annual direct incident radiation and heat load. Journal of Vegetation Science 13:603–606.

Meigs, G. W., H. S. J. Zald, J. L. Campbell, W. S. Keeton, and R. E. Kennedy. 2016. Do insect outbreaks reduce the severity of subsequent forest fires? Environmental Research Letters 11:045008.

Millar, C. I., and N. L. Stephenson. 2015. Temperate forest health in an era of emerging megadisturbance. Science 349:823–826.

Miller, J. D., E. E. Knapp, C. H. Key, C. N. Skinner, C. J. Isbell, R. M. Creasy, and J. W. Sherlock. 2009. Calibration and validation of the relative differenced normalized burn ratio (RdNBR) to three measures of fire severity in the Sierra Nevada and Klamath Mountains, California, USA. Remote Sensing of Environment 113:645–656.

Miller, J. D., C. N. Skinner, H. D. Safford, E. E. Knapp, and C. M. Ramirez. 2012. Trends and causes of severity, size, and number of fires in northwestern California, USA. Ecological Applications 22:184–203.

Miller, J. D., and A. E. Thode. 2007. Quantifying burn severity in a heterogeneous landscape with a relative version of the delta normalized burn ratio (dNBR). Remote Sensing of Environment 109:66–80.

Morgan, P., R. E. Keane, G. K. Dillon, T. B. Jain, A. T. Hudak, E. C. Karau, P. G. Sikkink, Z. A. Holden, and E. K. Strand. 2014. Challenges of assessing fire and burn severity using field measures, remote sensing and modelling. International Journal of Wildland Fire 23:1045.

Moritz, M. A., M.-A. Parisien, E. Batllori, M. A. Krawchuk, J. Van Dorn, D. J. Ganz, and K. Hayhoe. 2012. Climate change and disruptions to global fire activity. Ecosphere 3:art49.

Ospina, R., and S. L. P. Ferrari. 2012. A general class of zero-or-one inflated beta regression models. Computational Statistics & Data Analysis 56:1609–1623.

Parks, S. A., G. Dillon, and C. Miller. 2014*a*. A new metric for quantifying burn severity: the relativized burn ratio. Remote Sensing 6:1827–1844.

Parks, S. A., C. Miller, C. R. Nelson, and Z. A. Holden. 2014*b*. Previous fires moderate burn severity of subsequent wildland fires in two large western US wilderness areas. Ecosystems 17:29–42.

Parks, S. A., L. M. Holsinger, M. H. Panunto, W. M. Jolly, S. Z. Dobrowski, and G. K. Dillon. 2018*a*. High-severity fire: evaluating its key drivers and mapping its probability across western US forests. Environmental Research Letters 13:044037.

Parks, S. A., L. M. Holsinger, M. Voss, R. Loehman, and N. Robinson. 2018*b*. Mean composite fire severity metrics computed with Google Earth Engine offer improved accuracy and expanded mapping potential. Remote Sensing 10:879.

Patterson, M. W., and S. R. Yool. 1998. Mapping fire-induced vegetation mortality using landsat thematic mapper data: a comparison of linear transformation techniques. Remote Sensing of Environment 65:132–142.

Peet, R. K. 2000. Forests and meadows of the Rocky Mountains. Pages 75–122 *in* M. G. Barbour and W. D. Billings, editors. North American terrestrial vegetation. Second edition. Cambridge University Press, New York, New York, USA.

Prichard, S. J., and M. C. Kennedy. 2014. Fuel treatments and landform modify landscape patterns of burn severity in an extreme fire event. Ecological Applications 24:571–590.

R Development Core Team. 2018. R: a language and environment for statistical computing. R Foundation for Statistical Computing, Vienna, Austria.

Rollins, M. G. 2009. LANDFIRE: a nationally consistent vegetation, wildland fire, and fuel assessment. International Journal of Wildland Fire 18:235.

Roy, D. P., L. Boschetti, and S. N. Trigg. 2006. Remote sensing of fire severity: assessing the performance of the normalized burn ratio. IEEE Geoscience and Remote Sensing Letters 3:112–116.

Schoennagel, T., T. T. Veblen, and W. H. Romme. 2004. The interaction of fire, fuels, and climate across Rocky Mountain Forests. BioScience 54:661.

Smith, A. M. S., J. U. H. Eitel, and A. T. Hudak. 2010. Spectral analysis of charcoal on soils: implications for wildland fire severity mapping methods. International Journal of Wildland Fire 19:976–983.

Smith, A. M. S., L. B. Lentile, A. T. Hudak, and P. Morgan. 2007. Evaluation of linear spectral unmixing and ΔNBR for predicting post-fire recovery in a North American ponderosa pine forest. International Journal of Remote Sensing 28:5159–5166.

Smith, A. M. S., et al. 2016. Towards a new paradigm in fire severity research using dose–response experiments. International Journal of Wildland Fire 25:158–166.

Stan Development Team. 2018. RStan: the R interface to Stan. https://cran.r-project.org/web/packages/rstan/vignettes/rstan.html

Stevens, J. T., B. M. Collins, J. D. Miller, M. P. North, and S. L. Stephens. 2017. Changing spatial patterns of stand-replacing fire in California conifer forests. Forest Ecology and Management 406:28–36.

Westerling, A. L. 2016. Increasing western US forest wildfire activity: sensitivity to changes in the timing of spring. Philosophical Transactions of the Royal Society B: Biological Sciences 371:20150178.

White, J. D., K. C. Ryan, C. C. Key, and S. W. Running. 1996. Remote sensing of forest fire severity and vegetation recovery. International Journal of Wildland Fire 6:125–136.

Whitman, E., M.-A. Parisien, D. K. Thompson, R. J. Hall, R. S. Skakun, and M. D. Flannigan. 2018. Variability and drivers of burn severity in the northwestern Canadian boreal forest. Ecosphere 9:e02128.

Woodcock, C. E., and A. H. Strahler. 1987. The factor of scale in remote sensing. Remote Sensing of Environment 21:311–332.

Supporting Information

Additional Supporting Information may be found online at: http://onlinelibrary.wiley.com/doi/10.1002/ecs2.2600/full